J Mater Sci: Mater Med (2010) 21:1927–1936
DOI 10.1007/s10856-010-4044-2

Physicochemical properties and cytotoxicities of Sr-containing biphasic calcium phosphate bone scaffolds

Guo Dagang · Xu Kewei · Liu Yaxiong

Received: 23 January 2010 / Accepted: 1 March 2010 / Published online: 10 March 2010

Abstract This study demonstrates a new biomaterial system composed of Sr-containing hydroxyapatite (Sr-HA) and Sr-containing tricalcium phosphate (Sr-TCP), termed herein Sr-containing biphasic calcium phosphate (Sr-BCP). Furthermore, a series of new Sr-BCP porous scaffolds with tunable structure and properties has also been developed. These Sr-BCP scaffolds were obtained by in situ sintering of a series of composites formed by casting various Sr-containing calcium phosphate cement (Sr-CPC) into different rapid prototyping (RP) porous phenol formaldehyde resins, which acted as the negative moulds for controlling pore structures of the final scaffolds. Results show that the porous Sr-BCP scaffolds are composed of Sr-HA and Sr-TCP. The phase composition and the macro-structure of the Sr-BCP scaffold could be adjusted by controlling the processing parameters of the Sr-CPC pastes and the structure parameters of the RP negative mould, respectively. It is also found that both the compressive strength (CS) and the dissolving rate of the Sr-BCP scaffold significantly vary with their phase composition and macropore percentage. In particular, the compressive strength achieves a maximum CS level of 9.20 ± 1.30 MPa for the Sr-BCP scaffold with a Sr-HA/Sr-TCP weight ratio of 78:22, a macropore percentage of 30% (400–550 μm in size) and a total-porosity of 63.70%, significantly higher than that of the Sr-free BCP scaffold with similar porosity. All the extracts of the Sr-BCP scaffold exhibit no cytotoxicity. The current study shows that the incorporation of Sr plays an important role in positively improving the physicochemical properties of the BCP scaffold without introducing obvious cytotoxicity. It also reveals a potential clinical application for this material system as bone tissue engineering (BTE) scaffold.

G. Dagang (✉) · X. Kewei
State Key Laboratory for Mechanical Behavior of Materials, School of Material Science and Engineering, Xi'an Jiaotong University, 710049 Xi'an, China
e-mail: guodagang@mail.xjtu.edu.cn

L. Yaxiong
State Key Laboratory for Manufacturing Systems Engineering, School of Mechanical Engineering, Xi'an Jiaotong University, 710049 Xi'an, China

1 Introduction

Due to source limitation of the autogenetic bone graft and immunologic rejection problem of the allergenic bone graft [1], bone tissue engineering (BTE) technique has become a crucial strategy to permanently repair bone defects. However, from the material point of view, no existing scaffold possesses excellent synergistic properties of high mechanical strength, suitable degradation rate, high porosity with well-connected macro-pores and excellent bioactivity [2–4], which constitutes the main challenge to the use of traditional biomaterials in BTE. Thus, the invention of new scaffolding material systems as well as new fabricating techniques are the most important demands in the BTE field.

Biphasic calcium phosphate (BCP) ceramics composed of hydroxyapatite (HA) and β-tricalcium phosphate (β-TCP) have been extensively studied in the past two decades [5–10]. By combination of the advantages of HA (e.g. excellent biocompatibility and bioactivity, and can be directly bonded to the host bone [11, 12]) and β-TCP (e.g. suitable degradation rate that matches the growth rate of newly formed bone [13]), BCP ceramics have been recently developed as an excellent starting material to prepare the BTE scaffold. Moreover, BCP ceramics showed excellent osteoinductivity, osteoconductivity,

bioactivity and biodegradability [14–17] according to in vitro physiochemical property examinations and in vivo biological evaluations. In the previous study [18], we developed a series of porous BCP scaffolds with controllable phase compositions, controllable macropore structures, and adjustable properties by sintering a series of mixtures consisted of calcium phosphate cement (CPC) and rapid prototyping (RP) porous negative mold. Although some improvements to the structure and properties of the BCP scaffold made in this study, the potential in further enhancing the biodegradation rate and the mechanical strength was limited by simply tuning the HA/TCP ratio and controlling the porosity of the BCP scaffold. Therefore, it is critical to significantly improve the degradation rate and the mechanical strength of the BCP scaffold in synergy in order to further enlarge their application potentials.

Several years ago, we reported a new Sr-containing CPC (Sr-CPC) system with a major product of nonstoichiometic Sr-containing HA (Sr-HA) ($Ca_{10-m-x}Sr_x\square_m(HPO_4)_y\ (PO_4)_{6-y}(OH)_{2-2m}\square_{2m}$, $0 < x < 1$, nSr-HA) [19]. Both the in vitro and in vivo experiments showed that the incorporation of Sr^{2+} not only improved the biocompatibility and bioactivity of the HA bone cement, but also increased its compressive strength (CS) and biodegradation rate [19–21]. Following our previous work, in the present study, we proposed and demonstrated a new Sr-containing (or Sr-incorporated) BCP system composed of Sr-HA and Sr-containing tricalcium phosphate (Sr-TCP). We used the nonstoichiometic Sr-CPC as the starting material instead of pure CPC and obtained a new functionalized Sr-containing BCP (Sr-BCP) scaffold with an easily controlled degradation rate and a higher mechanical strength. To our knowledge, so far, such a Sr-BCP material and BTE scaffold system have not yet been reported elsewhere. The major work herein was to firstly characterize the phase composition, pore structure and in vitro physicochemical properties and cytotoxicity of the newly fabricated Sr-BCP scaffolds, as well as to intensively investigate the variations of in vitro mechanical strength and the dissolving rate as functions of major processing parameters.

2 Materials and methods

2.1 Cement and RP negative mould

The starting materials were as-prepared Sr-CPC with different (Ca + Sr)/P molar ratios. The Sr-free CPC with different Ca/P molar ratios were also used as a control. The cement powder mixture of Sr-CPC was composed of tetracalcium phosphate monoxide ($Ca_4(PO_4)_2O$, TTCP), strontium hydrogen phosphate ($SrHPO_4$, DSPA) and dicalcium phosphate anhydrous ($CaHPO_4$, DCPA) with a fixed molar ratio of 2:1:1, while that of the Sr-free CPC was composed of TTCP and DCPA with a fixed molar ratio of 1:1. TTCP was prepared by heating a mixture of DCPA and calcium carbonate ($CaCO_3$, CC) in a Ca/P ratio of 2.0, followed by a sintering step at 1500°C for 15 h in a furnace [22], where the heating units were silicomolybdic rods. Subsequently, the heated mixture was quenched to room temperature in a desiccator. The as-prepared product, determined by X-ray Diffraction (XRD) analysis, was pure TTCP with a high crystallinity. The TTCP particles were crushed by using mortar and pestle and then wetly ball-milled for 10 h with absolute ethyl alcohol as liquid medium. The mean size of the ground TTCP particles is 13 ± 2.4 μm. The apparatus was planet ball-milling machine (Nanjing University instrument corp., China). The milling conditions were as follows: balls (100 smaller balls in Φ5 and 15 larger balls in Φ10 used for each milling) and vial (200 ml in volume capacity) were made of alundum (Al_2O_3) and nylon, respectively; the total mass and average granularity of the raw powders were 50 g and 30–50 μm, respectively; the rotation speed was set at 400 rpm. DCPA was prepared by baking commercial dicalcium phosphate dihydrate ($CaHPO_4{\cdot}2H_2O$, DCPD) in oven at 120°C beyond 10 h. The baked DCPA was grounded with a wet ball-milling process similar to the one described above, except for a longer milling time (30 h) in order to obtain a finer powder (1 ± 0.2 μm). The $SrHPO_4$ powder was synthesized with a precipitation method, in which the precursors, $Sr(NO_3)_2$ and $(NH_4)HPO_4$, were mixed at pH = 7.0 [23]. The deposit sediments were washed by centrifuging with deioned water at least thrice and absolute ethyl alcohol at least twice, and then dried in oven at 80°C for at least 10 h. The obtained block of DSPA was crushed first by mortar and pestle and further ground for 30 h. The mean size of the obtained DSPA powders was 6.3 ± 1.2 μm. The liquid phase in the cement paste was deionized water or diluted phosphate acid. The concentrations of the latter were in the range of 0.40–0.75 M. Since the molar ratio of various phosphate salts in the cement powder mixture of Sr-CPC or Sr-free CPC was fixed, the (Ca + Sr)/P or Ca/P ratio that determines the phase composite of the final product could be adjusted by controlling the concentration of diluted phosphate acid and the weight ratio of powder to liquid (P/L). The details of the designed (Ca + Sr)/P or Ca/P ratio are summarized in Table 1.

Rapid prototyping is an advanced manufacturing technique and is advantageous for making complex prototypes [18, 24]. The RP technique is a modeling process used in product design in which a computer-aided design (CAD) drawing of a component is processed to create a file of the component in slices, and then the slices are used to direct the layer-by-layer construction of the component through various material deposition steps; including stereolithography,

Table 1 Designed and actually obtained phase compositions of Sr-BCP scaffolds

Sample	Designed composition ((Sr-)HA: (Sr-TCP, wt%)	Theoretical Ca/P or (Ca + Sr)/P molar ratio	Concentration of H_3PO_4 solution (mol/l)	Actual composition ((Sr-)HA: (Sr-)TCP, wt%)
Sr-BCP1	25:75	1.5393	0.75	30:70
Sr-BCP2	75:25	1.6226	0.40	78:22
Sr-BCP3	100:0	1.6667	0[a]	99.5:0.5
BCP1[b]	25:75	1.5393	0.75	32:68
BCP2[b]	75:25	1.6226	0.40	83:17
BCP3[b]	100:0	1.6667	0[a]	99:1

[a] The deioned water

[b] Sr-free BCP samples reported previously [18] were listed here as controls

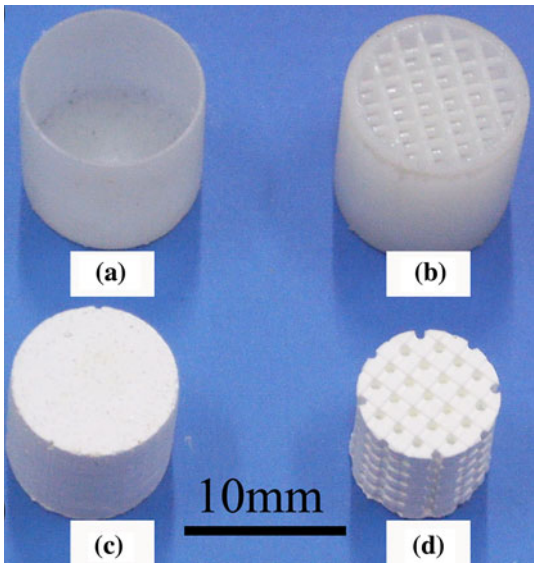

Fig. 1 The RP phenol formaldehyde resin negative moulds (RP mould) and the obtained scaffolds with different macropore percentages (P_{macro}): **a** RP mould, $P_{macro} = 100\%$; **b** RP mould, $P_{macro} = 70\%$; **c** Scaffolds, $P_{macro} = 0\%$; **d** Scaffolds, $P_{macro} = 30\%$

selective laser sintering, or fused deposition modeling. In this experiment, we used the RP technique to make the structure-controlled 3D porous negative moulds from a raw material of phenol formaldehyde resins [18]. Figure 1a and b shows two as-prepared negative moulds with designed macroporosity percentages of 100 and 70%, respectively. The inner-diameter, height and macropore wall diameter (or mesh-rod diameter) of the negative moulds were Φ10.5 mm, 17 mm and Φ600 μm, respectively.

2.2 Casting and hydration of cement pastes

After mixing the cement powder mixture with the liquid phase for 30 s, the obtained cement pastes were cast into the negative mould. The paste-containing mould was shaken frequently but lightly to release the air bubbles that had been mixed into the pastes during the casting process. For more a convenient description, we term the negative mould filled with the cement pastes the "mould/cement composite".

2.3 Negative mould removing and scaffold sintering routes

The establishment of an appropriate negative mould removing and scaffold sintering route is quite critical to the final phase composition, crystallinity and physicochemical properties of the obtained ceramics. Based on the results from thermo-gravimetric analysis (TGA) and differential scanning calorimetry (DSC) obtained on the negative mould resin reported previously [18], we chose a similar route to remove the negative mould and further sinter the initially formed scaffold: firstly, the samples were heated from room temperature to 400°C at an increment of 0.5°C/min and then held constant at 400°C for 2 h for complete removal of the negative mould; secondly, the initially formed scaffolds were heated to 1200°C at an increment of 1.0°C/min and again held constant for 4 h at 1200°C to achieve effective sintering; finally, the scaffolds were in situ cooled from 1200°C to a temperature below 100°C in the furnace.

2.4 CS measurements

All samples prepared for mechanical property characterization were slightly polished with fine abrasive paper (1200 no.). To keep depths of both parallelism and verticality of the samples, a special self-designed clamping fixture was used to fix the sample during polishing. CS values were measured by using a computer-controlled Universal Testing Machine (WDW-1000, Hua-Long Corp., China). The cross-head speed was controlled at 0.5 mm/min with a special consideration for the dimension of the tested samples and the loading-displacement curve was recorded by the computer. A mean CS value was determined using at least five parallel samples prepared under the same conditions.

2.5 In vitro evaluation on the degradation rate

A series of static immersion experiments were preformed in physiological saline (0.9% NaCl solution) for evaluating the degradation (or dissolving) rates of various samples. Each sample was immersed in the physiological saline strictly according to a reference of 50 ml solution per gram sample. The immersion time of the samples was 4w, 6w, 8w, 10w, 12w, 14w and 16w, respectively and the immersion temperature was kept at 37°C. Every 3 days, the immersion solution was renewed. After the preset immersion time was reached, the immersed samples were taken out of the physiological saline and dried according to the following steps: firstly, the immersed samples were predried in a regular oven at 80°C for 5 h; secondly, the samples were placed into an ultra-vacuum chamber coupled with JGP560C magnetron sputtering device and maintained for 5 h under the conditions of 90 ± 1°C and 1.0–1.2 × 10^{-3} Pa. The dried samples were weighed by an electronic balance (CP214, America Ohaus, Shanghai, China) with a precision of 0.1 mg.

2.6 Porosity determination

The porosity of the Sr-BCP scaffolds was indirectly evaluated by a method similar to one proposed by Takagi and Chow [25]. In this method, the total porosity (*P*total) of a specimen was calculated according to the following equation:

$$P_{\text{total}} = \left(1 - d_{\text{apparent}}/d_{\text{Sr-BCP}}\right) \times 100\% \quad (1)$$

where d_{apparent} is the apparent density of the dried specimen, calculated by immersion in Hg with the Archimedes principle, and *d*Sr-BCP is the theoretical density of the Sr-BCP ceramic calculated from the mixture rule [18] using the corresponding density data of different phases with the assumption of volume conservation (see Eq. 2):

$$d_{\text{Sr-BCP}} = (d_{\text{Sr-HA}} \cdot d_{\text{Sr-TCP}})/(\delta \cdot d_{\text{Sr-TCP}} + (1-\delta) \cdot d_{\text{Sr-HA}}) \quad (2)$$

where δ is the weight percentage of Sr-HA in the Sr-BCP ceramic, and the theoretical densities of Sr-HA and Sr-TCP were *d*Sr-HA = 3.247 g/cm^3 and *d*Sr-TCP = 3.222 g/cm^3, respectively, calculated by immersion in Hg with the Archimedes principle for each pure fine powder phase.

The microporosity (*P*micro) of the Sr-BCP ceramic without any macro-pore is just the *P*total calculated by Eq. 1, and the *P*micro of the Sr-BCP ceramic with a designed macroporosity (*P*macro) is calculated according to the following equation:

$$P_{\text{micro}} = P_{\text{total}} - P_{\text{macro}} \quad (3)$$

It should be noted that the Eq. 3 was based on an assumption that volume variation of the resin mould during the sintering was negligible.

2.7 Characterization methods

Phase compositions of the samples in the form of powders were determined via XRD with Cu-K_α radiation and Ni filter. The electrical voltage and current settings were 35 kV and 30 mA, respectively. Fractured surfaces of the samples were observed with scanning electron microscopy (SEM, JSM6460, Japan). Energy dispersive X-ray spectroscopy (EDXS) coupled with the SEM device was used to characterize chemical elements in the various samples.

2.8 Cytotoxicity procedure

Cytotoxicity tests were performed by adding different dilutions of powder sample extract to a L929 cell culture on a 96-well plate. In this experiment, the L929 cells isolated from mice were provided by the Fourth Military Medical University, China. The powder samples were obtained via a grinding process described as follows: the scaffold samples had firstly been dried at 50°C for 1 h, and then the dried samples were crushed in a porcelain mortar and sieved through a no. 100 mesh ASTM sieve with a pore size of 150 μm. A total six sample groups including BCP1, BCP2, BCP3, Sr-BCP1, Sr-BCP2 and Sr-CP3 were compared in the cytotoxicity test. The positive and negative controls used were 6.4 M phenol solution and free-culture, respectively. In each group, five samples under the same conditions were tested to obtain a mean value.

2.8.1 Preparation of extracts

1.5 g of each sample, sterilized by gamma radiation (25 kGy), was added to its own corresponding 100 ml glass flasks loaded with 15 ml DMEM-BFS culture medium containing 10% (vol/vol) of bovine fetal serum (pH = 7.2). A total of six flasks were simultaneously incubated in a humid atmosphere of 5% CO_2 at 37°C for 7 days. After incubation, the supernatant was filtered through a membrane and then serial dilutions of 100, 50, 10, and 5% (vol/vol) pure extract were prepared, respectively.

2.8.2 Preparation of cell strain

The L929 cells were cultivated with DMEM-BFS medium in an incubator at 37°C with a humid atmosphere of 5% CO_2. Before starting the experiment, the cells were washed with a calcium and magnesium free saline phosphate buffer

(PBS-CMF). Subsequently, cells were detached using a 2.5 g/l trypsin solution and then re-suspended in DMEM-BFS. Finally, the suspension was adjusted to 1×10^4 cells/ml and inoculated on a 96-well plate and the plate was incubated for cell adhesion with 200 μm of suspension per well.

2.8.3 *Cytotoxicity testing-MTT assay*

After seeding in 96-well plate and incubating for 24 h, the culture medium was removed and the dilutions and controls previously prepared were added into the wells for inoculating L929 cells. Each concentration of tested extracts was made in six duplicates. The plate was incubated in a humid incubator with 5% CO_2 at 37°C for 72 h, after which 20 μl methyl thiazoly tetrazolium (MTT) solution of 5 g/l was added into each well in the plate and incubation was continued for 4 h under the same condition. Thereafter, the supernatant of each well was carefully aspirated and replaced with 150 μl dimethyl sulfoxide (DMSO), followed by 10 min shaking. A DG3022 Enzyme Linked Immunosorbent Machine with a wavelength of 490 nm was used to determine the optical absorption data (OD) of each well, which was used to calculate the relative growth rate (RGR) of L929 cells using the following equation.

$$\mathrm{RGR}\,(\%) = \mathrm{OD\ of\ tested\ sample}/\mathrm{OD\ of\ negative\ control} \quad (4)$$

2.9 Statistical analysis

The present study made an analysis of variance in discussing the influences of some parameters on physicochemical properties and cytotoxicity of the scaffold samples by using the Procanova Procedure in SAS system. The family confidence coefficient (cc) was given to be 0.95.

3 Results

Figure 2 shows the XRD patterns of various samples with different (Ca + Sr)/P ratios after sintering at 1200°C for 4 h. Both the relative intensity and angle corresponding to each diffraction peak of Sr-BCP3 (see Fig. 2a) matches very well with those in the standard JCPDS card of $SrCa_9(PO_4)_6 2OH$ (10% Sr-HA). As the (Ca + Sr)/P molar ratio in the starting materials (see Table 1) decreases, the relative intensity corresponding to each diffraction peak of 10% Sr-HA gradually decreases, but the new diffraction peaks (mainly located at 27.73°, 30.98°, 34.27°, etc.) corresponding to the diffraction patterns of Sr-β-TCP [26] increases (see Fig. 2b, c). Through a further quantitative XRD analysis with an equipped analysis program, weight ratios of Sr-HA-like phase to Sr-β-TCP-like phase in all the

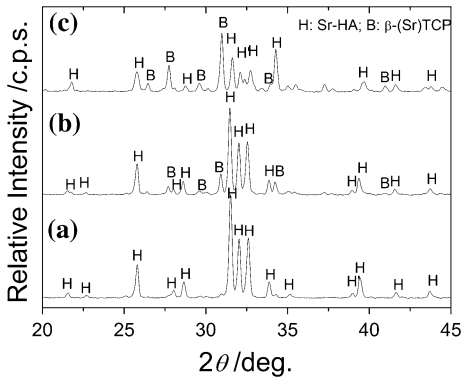

Fig. 2 XRD patterns of various scaffold samples sintered at 1200°C for 4 h. *a* Sr-BCP3, *b* Sr-BCP2, *c* Sr-BCP1

tested samples were obtained (the last column of Table 1, which shows that the actual phase composites of the sintered products are consistent to those of the designed ones). In general, the results obtained here indicate that the final composition of the sintered products could be easily adjusted by changing the (Ca + Sr)/P molar ratio of the starting materials (Sr-CPC). It also suggests a potential easily controlled industrialization process.

The typical digital images of the Sr-BCP samples containing with 0 and 30% macroporosity were shown in Fig. 1c and d, respectively. One can see that the porous scaffold containing 30% macroporosity displayed an intact profile. By comparing with our previous work on Sr-free BCP [18], it is clear that the introduction of Sr into phase composition of the final products did not yield significant effect on the macrostructure of the obtained scaffold, except that the macropore sizes of Sr-BCP scaffold (450–600 μm, see Fig. 3a) were slightly larger than those of Sr-free BCP scaffold (Φ400–500 μm). After further enlarging the surface of the macropore walls (Fig. 3b–d), it was found that many micropores with sizes in the range of 2–5 μm were distributed in the macropore wall of the Sr-BCP scaffold, which was also similar to those of the Sr-free BCP scaffold reported previously [18]. In addition, the macropore wall of the Sr-BCP scaffolds exhibited two typical crystal morphologies. To further identify these two crystal phases, their EDX spectra were measured and the results are shown in Fig. 3e and f. From the results of EDX spectra analysis (see Table 2), the (Ca + Sr)/P ratio of irregular ring-like particles corresponding to site "1" was approximately 1.49 while the one of the equiaxial-like particle corresponding to site "2" was approximately 1.71. Based on the above XRD results, it can be speculated that the irregular ring-like particles and the equiaxial-like particles were Sr-TCP and Sr-HA, respectively. Furthermore, when the (Ca + Sr)/P ratio increased from 1.54 to 1.67 (see Fig. 3b–d), the number of irregular ring-like particles gradually decreased but that

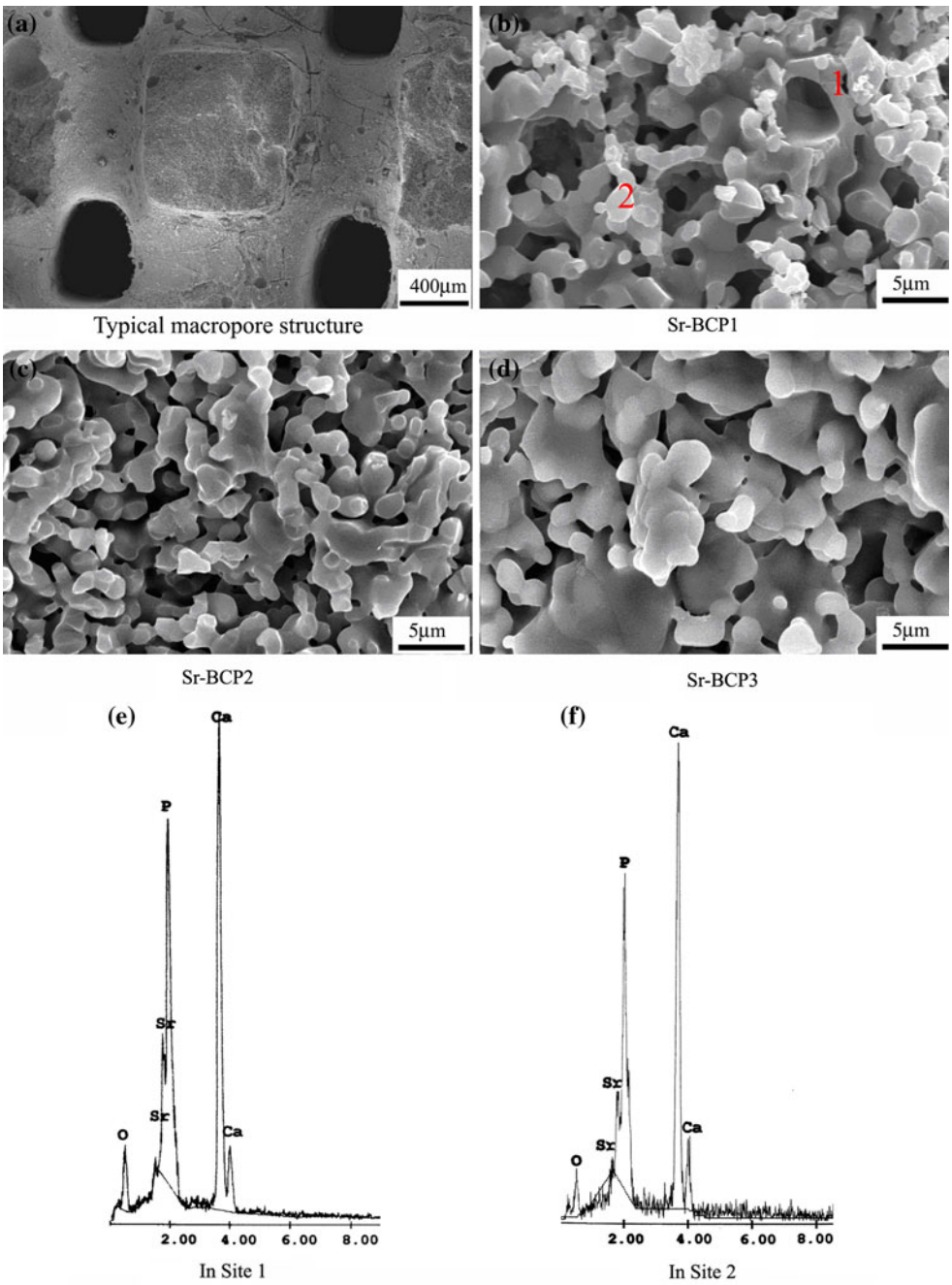

Fig. 3 The scanning electron micrograph (SEM) images of macropore structure (macroporosity = 30%) (**a**) and micropore structures (in the macropore wall) (**b**–**d**) of the Sr-BCP scaffolds with different Sr-HA/Sr-TCP ratios, and the EDX spectra (**e**, **f**) of the typical particles in site 1 and site 2 marked in the SEM photographs (**b**)

of the equiaxial-like particle increased correspondingly. Interestingly, the Sr-HA particles tended to fuse in the absence of the second phase (Sr-TCP). In summary, the final Sr-containing scaffold is composed of Sr-HA and Sr-TCP with approximate formulas of $Ca_{2.6}Sr_{0.4}(PO_4)_2$ and $Ca_9Sr(PO_4)_6(OH)_2$, respectively. Hereby, we specially term them as Sr-containing biphasic calcium phosphate or Sr-BCP compared with the well-known pure BCP.

Figure 4 shows the CS values of the Sr-BCP samples at various phase compositions and macropore percentages. The CS values of the Sr-BCP scaffolds with a 30% macroporosity were significantly lower than those of the Sr-BCP samples without macropores. With increasing Sr-HA content, the CS values of both the Sr-BCP scaffolds

Table 2 The corresponding analyses results of the EDX spectra in Fig. 3

Sites	Phase composition	Sr/(Ca + Sr)	(Ca + Sr)/P	Estimated formula
1	Sr-TCP	0.13	1.49	$Ca_{2.6}Sr_{0.4}(PO_4)_2$
2	Sr-HAP	0.10	1.71	$Ca_9Sr(PO_4)_6(OH)_2$

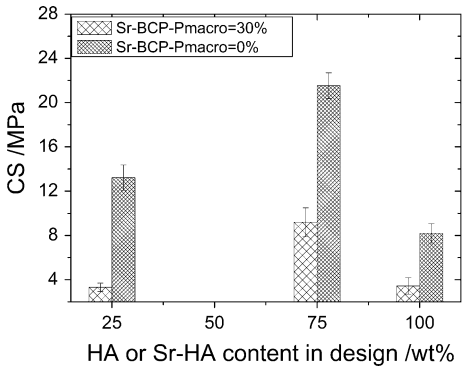

Fig. 4 Compressive strength (CS) values of various Sr-BCP scaffolds with different phase compositions and macropore percentages

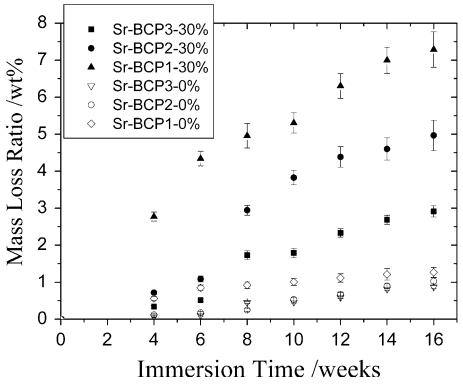

Fig. 5 The mass loss ratios of the Sr-BCP scaffolds containing 0 and 30% macropores, respectively, at various immersion stages

containing 30 and 0% macropores first increased but then decreased (cc = 0.95). This trend is extremely similar to the Sr-free BCP samples reported elsewhere [18]. It indicates that both the macropore percentage and the phase composition play important roles in the CS values of the Sr-BCP samples. It is noteworthy that the CS value of the Sr-BCP scaffold containing a designed macropore percentage of 30% and a designed Sr-HA/Sr-TCP weight ratio of 75:25 was 9.20 ± 1.30 MPa, significantly higher than that of the Sr-free scaffold (4.55 ± 0.92 MPa) [18] at the same designed parameters (cc = 0.95). This result reveals that the substitution of Ca by equivalent Sr greatly improves the mechanical strength of the BCP scaffold.

Table 3 summarized the macro- and micro-pore percentages of various Sr-BCP samples. A considerable micro-porosity of 42.75–44.23% was found in the Sr-BCP samples without designed macropores, according to the SEM images of the microstructure on the surface of the macropore wall (see Fig. 3b–d). These micropores are mainly the result of from capillary pores generated in the hydration process of Sr-CPC [19]. Due to the existence of these micropores, the actual total porosities of the Sr-BCP scaffolds containing 30% macropores were in range of 61.85–63.70%.

Obtained from a preliminary in vitro evaluation on the degradation rate of the Sr-BCP materials, Fig. 5 shows mass loss ratios of various Sr-BCP samples containing 0 and 30% macropores, respectively, at various immersion stages in physiological saline (0.9% NaCl solution). It was found that the mass loss ratios of all the Sr-BCP scaffolds increase almost linearly as extending the immersion time. Moreover, with the decrease of the Sr-HA/Sr-TCP ratio, the mass loss ratios of the Sr-BCP scaffolds increased remarkably (cc = 0.95), indicating that the dissolving rate of the Sr-TCP is higher than that of the Sr-HA. The mass loss ratio of any Sr-BCP scaffold containing designed 30% macropores is significantly higher than that of the Sr-BCP sample without macropore. It indicates that the introduction macropores into Sr-BCP scaffolds significantly accelerates their dissolving rate. In addition, with the same Sr-HA/Sr-TCP ratio, the degradation rates of Sr-BCP scaffolds at various immersion stages were much faster than those of Sr-free BCP scaffolds [18] (cc = 0.95). More interestingly, the dissolution rate of Sr-BCP3 scaffold with a designed Sr-HA/Sr-TCP ratio of 100:0 (wt%:wt%) (i.e. pure Sr-HA scaffold) is even larger than that of the Sr-free BCP scaffold with a designed HA/TCP ratio of 25:75 (wt%:wt%). Based on the above results, the degradation rate order of these scaffolds can be initially summarized as follows:

$$\begin{aligned}&\text{Sr-TCP} > \text{Sr-BCP} > \text{Sr-HA} > \\ &\text{BCP (TCP : HA} < 75\,\text{wt\%} : 25\,\text{wt\%}) > \text{HA}\end{aligned} \tag{5}$$

Figure 6 shows the percentages of RGR of L929 cells incubated in different serial extracts of various Sr-BCP and Sr-free BCP samples. For all the tested samples, the RGR values of L929 cells in the extracts with lower concentration are slightly larger than those corresponding to the higher concentrations. In particular, the mean RGR value of L929 cells in the 5 wt% pure extract for any tested samples is statistically (cc = 0.95) larger than that of L929 cells in the 100 wt% pure extract. This is extremely similar to the cytotoxicity result reported elsewhere [19] for the Sr-CPC materials. Moreover, except for the slightly lower RGR values of the Sr-BCP3 extracts with higher concentrations, there were almost no significant difference

Table 3 The total porosity (*P*total), macropore percentage (*P*macro) and micropore percentage (*P*micro) of various Sr-BCP scaffolds

Sample codes (%)	*P*total (%)	*P*macro (%)	*P*micro (%)
Sr-BCP1-0	42.75	0	42.75
Sr-BCP2-0	44.06	0	44.06
Sr-BCP3-0	44.23	0	44.23
Sr-BCP1-30	62.01	30	32.01
Sr-BCP2-30	63.70	30	33.70
Sr-BCP3-30	61.85	30	31.85

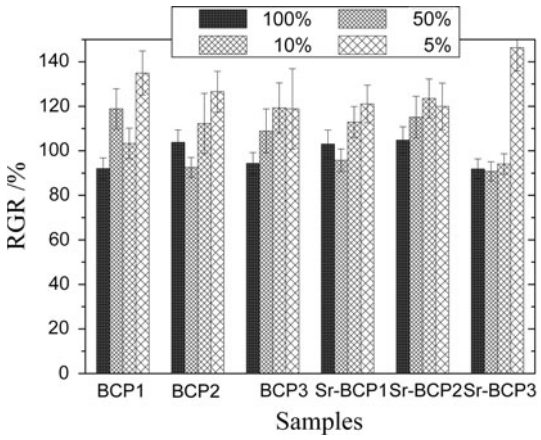

Fig. 6 The relative growth rate (RGR) percentages of L929 cells incubated in various scaffold extracts

observed between the RGR value of L929 cells in the extracts of each Sr-BCP sample and that of the corresponding BCP sample at the same concentration (cc = 0.95). As a whole, all extracts exhibit no or low cytotoxicity with a score of 0 or 1 grade according to the six-grade criterion of Chinese National Standard for Medical Devices and Implants—GB/T 16175-1996 [27]. It implies that the Sr-BCP scaffolds possess an excellent biocompatibility similar to the BCP scaffold.

4 Discussions

With the rapid development of BTE, great progress has been made in the last decade. However, as advancements are made, new challenges also emerge, which comes from the crucial clinical requirements on the bone scaffolding materials [2–4]. Currently, the critical issue of concern for a newly developed scaffold is how to simultaneously achieve its higher mechanical strength, moderate degradation rate, higher porosity, and reasonable pore size distribution. BCP is an important candidate of the bone scaffold material that combines higher mechanical strength, excellent bioactivity of HA, and faster degradation rate of TCP [15]. However, our previous study [18] implied that there was still a limitation in further increasing the degradation rate and mechanical strength of the BCP scaffold with a high porosity in order to meet the clinical requirements. Here, based on the fact that Sr-HA phase has stronger mechanical strength and faster degradation rate than pure HA [19, 21], we introduced Sr into BCP to generate a novel Sr-containing BCP scaffold composed of Sr-HA and Sr-TCP.

In the present study, various Sr-containing BCP scaffolds were successfully in situ prepared by using Sr-CPC as the casting material and RP porous resin as the structure-controlled negative mould. The final composition (i.e. the weight ratio of Sr-HA to Sr-TCP) could be adjusted by varying the (Ca + Sr)/P ratio of the Sr-CPC. The CS value of the Sr-BCP scaffold with a designed Sr-HA/Sr-TCP ratio of 75:25 (wt%:wt%) and a total porosity of 63.70% reached 9.20 ± 1.30 MPa, approximately twofolds of the Sr-free BCP scaffold (4.55 ± 0.92 MPa) at the same designed parameters (cc = 0.95). Moreover, the CS level of the Sr-BCP scaffold is significantly higher than common CS levels (~5 MPa) of the other existing porous BTE scaffold at the similar porosity [28, 29] and is comparable to the higher end in CS value of human cancellous bone (2–12 MPa) [30–32]. This is indication that the Sr-BCP scaffold can be used in human cancellous BTE where the cancellous bone defects are mainly distributed at relative higher load-bearing sites, such as at vertebra, fumer, tibia, etc. In addition, according to the results of Figs. 4 and 5, both mechanical strength and degradation rate of the Sr-BCP scaffold could be further adjusted according to the actual needs of the repaired site by altering their Sr-HA/Sr-TCP weight ratio and macropore percentage. Under the same conditions, not only is the mechanical strength of the Sr-BCP scaffold higher than that of the BCP scaffold, but the degradation rate of the Sr-BCP scaffold is also faster than that of the BCP scaffold. Clearly, the incorporation of Sr into BCP significantly improves both mechanical strength and degradation rate. Therefore, the present results match our original concept very well in further increasing the degradation rate and mechanical strength of the BCP scaffold by the incorporation of Sr. It has been well reported that the substitution of Sr for Ca significantly increases the mechanical strength as well as the degradation rate of HA [19, 21, 33], which might be one of the major contributors to the favorable variations in mechanical strength and degradation rate of the Sr-BCP. However, up to now, the underlying mechanisms have not yet been clarified. Someone researchers speculated that the increase in mechanical strength and degradation rate of HA might be related to its chemical strengthening [34] and crystal distortion or crystal defect [35] during the Sr incorporation, but there is no sufficient data to support this explanation. The influence of Sr incorporation on the mechanical strength and degradation rate of TCP and their mechanisms need to be further studied in the future.

Besides the mechanical strength and degradation rate, the pore-structure including micropore or macropore is another important characteristic for a prospective scaffold. It is still under debate which ranges of macropore diameter and macropore percentage in a would-be scaffold are desirable to facilitate bone ingrowth [15, 16, 36–42]. Gauthier et al. [15] investigate this issue on BCP scaffolds for bone ingrowth. His results showed the BCP scaffolds with 565 μm macropore size provided more abundant newly formed bone than those with 300 μm macropore

size, and none significant difference in bone formation amount was observed between the implants with 40 and 50% macropore percentage. Given the medium diameter of human osteon is approximately 223 μm [43, 44], we speculate that the suitable diameter of macropore should be in range of 400–600 μm. Therefore, the Sr-BCP scaffolds gained in this study also possess a suitable macropore size (500–600 μm) and macropore percentage (30%) which facilitates ingrowth of newly formed bone.

Our results also show that the Sr-BCP scaffold with a macropore structure inversely adjusted by the RP negative mould achieves its high interconnectivity. Other than the 30% designed macropores (500–600 μm), the Sr-BCP scaffold possesses another 41.85–44.70% micropores (2–5 μm). As a matter of fact, these micropores distributed in the macro-pore wall with a size of several micrometers are quite beneficial to promote circulation of body fluids, material resorption and bone substitute in vivo [45], and also was considered to be prerequisite for possessing excellent in vivo osteoinduction of the Ca–P materials [46–49]. Therefore, the present Sr-BCP scaffold possesses an excellent macropore and micropore structure in consideration for osteoconductivity and osteoinduction.

Although the RGR of L929 cells is slightly influenced by weight ratio of Sr-HA to Sr-TCP and concentration of its extract, the Sr-BCP scaffolds exhibit no cytotoxicity. The initial result provides an important proof to necessitate further investigations on other biocompatibility tests and animal experiments. It is also noted that applying the RP technique to prepare the negative mould not only achieves the higher macropore interconnectivity but also ensures higher repeatability in processing the Sr-BCP scaffolds. In future work, a real biomimetic bone scaffold similar to natural bone can be expected by further developing the RP technique, nature bone structure study and computer program related to bone structure analysis.

5 Conclusions

A new Sr-BCP scaffold composed of Sr-HA and Sr-TCP was firstly prepared by combining CPC and RP negative mould. The Sr-BCP scaffold displayed variable phase compositions, controllable macropore structures and also adjustable properties including mechanical strength and degradation rate. In comparison with Sr-free BCP scaffold, the CS of the Sr-BCP scaffold was remarkably enhanced and its degradation rate was significantly increased, which overcame the difficulty in simultaneously achieving higher mechanical strength and faster degradation rate in BCP scaffold. Also, the Sr-BCP materials did not show little or no cytotoxicity. In summary, this study provides some evidence that Sr incorporation to the physicochemical properties and cytotoxicity of BCP bone scaffold and the development of the Sr-BCP is one of important promotions to the traditional BCP, just as Sr-HA is an important promotion to the HA. It also indicates that this Sr-BCP material would possesses potential for clinical applications in both BTE and direct bone defect repairing. The future work would be to design the biomimetic bone scaffold and also to study the influence mechanisms of Sr incorporation on both HA and TCP.

Acknowledgements This work was supported by the National Natural Science Foundation of China (No: 50702043), Ph.D. Program Foundation of Ministry of Education of China (20070698092) and Program for New Century Excellent Talents in Universities (Chinese Ministry of Education, 2301G107aaa). The authors would like to thank Mr. Wang Wei, a graduate student of the Fourth Military Medical University, for his help to perform the cytotoxicity test. The authors also appreciate the help of Dr. Chenjie Xu and Ms. Luye Mu (Harvard-MIT Division of Health Science & Technology) for correcting grammar and language.

References

1. Goldberg VM, Stevenson S. Bone graft options: fact and fancy. Orthopedics. 1994;17:809–10.
2. Hollister SJ. Scaffold design and manufacturing: from concept to clinic. Adv Mater. 2009;21:3330–42.
3. Karen JLB, Scott P, James FK. Biomaterial developments for bone tissue engineering. Biomaterials. 2000;21:2347–59.
4. Dietmar WH. Scaffolds in tissue engineering bone and cartilage. Biomaterials. 2000;21:2529–43.
5. Dacilsi G, Legeros RZ, Nery E, et al. Transformation of biphasic calcium phosphate ceramics in vivo: ultrastructural and physicochemical characteristics. J Biomed Mater Res. 1989;23:883–94.
6. Piattelli A, Scarano A, Mangano C. Clinical and histologic aspects of biphasic calcium phosphate ceramic (BCP) used in connection with implant placement. Biomaterials. 1996;17:1767–70.
7. Curran JM, Grallagher JA, Hunt JA. The inflammatory potential of biphasic calcium phosphate granules in osteoblast/macrophage co-culture. Biomaterials. 2005;26:5313–20.
8. Daculsi G, Martin S, Martin S. Macroporous biphasic calcium phosphate ceramic for long bone surgery in human and dogs: clinical and histological study. J Biomed Mater Res A. 1990;24:379–96.
9. Lu XF, Lu B, Zhang J, et al. Osteogenesis of HA/TCP biphasic ceramics implanted into muscle: a long-term study. J Biomed Eng. 2002;19(3):361–4.
10. Legeros RZ, Lin S, Rohanizadeh R, et al. Biphasic calcium phosphate bioceramics: preparation, properties and applications. J Mater Sci Mater Med. 2003;14:201–9.
11. Ducheyne P, de Groot K. In vivo surface activity of a hydroxyapatite alveolar bone substitute. J Biomed Mater Res. 1981;15:441–5.
12. Aoki H. Medical application of hydroxyapatite. St. Louis: Ishiyaku Euro America; 1994. p. 13–75.
13. Roger F, Nathalie R, Philippe B. Preparation of α- and β-tricalcium phosphate ceramics, with and without magnesium addition. Ceram Int. 1994;20(5):327–36.
14. Arinzeh TL, Tran T, Daculsi G, et al. A comparative study of biphasic calcium phosphate ceramics for human mesenchymal stem-cell-induces bone formation. Biomaterials. 2005;26:3631–8.

15. Gauthier O, Bouler JM, Aguado E, et al. Macroporous biphasic calcium phosphate ceramics: influence of macropore diameter and macroporosity percentage on bone ingrowth. Biomaterials. 1998;19(3):133–9.
16. Eggli PS, Muller W, Schenk RK. Porous hydroxyapatite and tricalcium phosphate cylinders with two different pore size ranges implanted in the cancellous bone of rabbits. Clin Orthop Relat Res. 1988;232:127–38.
17. Yuan HP, Van Blitterswijk CA, De Groot K, De Bruijn JD. Cross-species comparison of ectopic bone formation in biphasic calcium phosphate (BCP) and hydroxyapatite (HA) scaffolds. Tissue Eng. 2006;12(6):1607–15.
18. Guo DG, Han Y, Xu KW, Luo F. The in situ synthesis of biphasic calcium phosphate scaffolds with controllable compositions, structures, and adjustable properties. J Biomed Mater Res. 2009; 88A:43–52.
19. Guo DG, Xu KW, Zhao XY, Han Y. Development of a strontium-containing hydroxyapatite bone cement. Biomaterials. 2005; 26(19):4073–83.
20. Guo DG, Xu KW, Yue J, Han Y, Zhao XY. pH value evolution of a novel Sr-containing calcium phosphate cement pastes and cytotoxicities of their hardened bodies. J Inorg Mater. 2005; 20(5):1159–66.
21. Guo DG, Xu KW, Han Y, Zhao XY. The influence of the Sr doses on the in vitro biocompatibility and in vivo degradability of the single-phase Sr-incorporated HAP cement. J Biomed Mater Res A. 2008;86A(4):947–58.
22. Guo DG, Xu KW, Han Y. Influence of cooling modes on purity of solid-state synthesized tetracalcium phosphate. Mater Sci Eng B. 2005;116(2):175–81.
23. Guo DG, Xu KW, Zhao XY, Sun HL, Han Y. Research on process of strontium hydrogen phosphate synthesized by chemical wet method. Rare Metal Mater Eng. 2005;34(5):799–802.
24. Woesz A, Rumpler M, Stampfl J, et al. Towards bone replacement materials from calcium phosphates via rapid prototyping and ceramic gelcasting. Mater Sci Eng C. 2005;25:181–6.
25. Takasi S, Chow LC. Formation of macropores in calcium phosphate cement implants. J Mater Sci Mater Med. 2001;12:135–9.
26. Lerous L, Lacout JL. Preparation of calcium strontium hydroxyapatites by a new route involving calcium phosphate cements. J Mater Res. 2001;16:171–6.
27. Chinese National Standard for Medical Devices and Implants—GB/T 16175-1996; 2003. p. 6–8.
28. Luo F, Guo DG, Han Y, Xu KW. Porous calcium phosphate scaffold prepared by foam immersion method. J Chin Ceram Soc. 2006;34(2):183–6.
29. Ramay HR, Zhang M. Preparation of porous hydroxyapatite scaffolds by combination of the gel casting and polymer sponge methods. Biomaterials. 2003;24:3292–302.
30. Giesen EBW, Ding M, Dalstra M, et al. Mechanical properties of cancellous bone in the human mandibular condyle are anisotropic. J Biomech. 2001;34:799–803.
31. Yeni YN, Fyhrie DP. Finite element calculated uniaxial apparent stiffness is a consistent predictor of uniaxial apparent strength in human vertebral cancellous bone tested with different boundary conditions. J Biomech. 2001;34:1649–54.
32. Gibson LJ. The mechanical behavior of cancellous bone. Biomechanics. 1985;18:317–28.
33. Christoffersen J, Christoffersen MR, Kolthoff N. Effects of strontium ions on growth and dissolution of hydroxyapatite and on bone mineral detection. Bone. 1997;20:47–52.
34. Chen DM, Fu YF. Evaluation on the mechanical properties of the solid solution of strontium-substituted hydroxyapatite. Chin J Stoma Mater Appar. 2001;19:178–83.
35. Chen DM, Fu Y, Gu GZ, et al. Preparation and solubility of the solid solution of strontium substituted hydroxyapatite. Chin J Biomed Eng. 2001;20(3):278–80.
36. Almirall A, Larrecq G, Delgado JA, et al. Fabrication of low temperature macroporous hydroxyapatite scaffolds by foaming and hydrolysis of an α-TCP paste. Biomaterials. 2004;25: 3671–80.
37. Kalita SJ, Bose S, Hosick HL, et al. Development of controlled porosity polymer-ceramic composite scaffolds via fused deposition modeling. Mater Sci Eng C. 2003;23:611–20.
38. Galois L, Mainard D, Bordji K, et al. Influence de la taille des pores sur la réhabitation osseuse de deux céramiques phosphocalciques: I'hydroxyapatite et le phosphate tricalcique. In: Editions Romillat, Actualités en biomatériaux, Paris; 1996, vol 3. p. 361–80.
39. Uchida A, Nade S, McCartney E, et al. Bone ingrown into three different porous ceramics implanted into the tibia of rats and rabbits. J Orthop Res. 1985;3:65–77.
40. Shimazaki K, Mooney V. Comparative study of porous hydroxyapatite and tricalcium phosphate as bone substitute. J Orthop Res. 1985;3:301–10.
41. Holmes RE, Bucholz RW, Mooney V. Porous hydroxyapatite as a bone graft substitute in diaphyseal defects: a histometric study. J Orthop Res. 1987;5:114–21.
42. Dacusi G, Passuti N. Effect of the porosity for osseous substitution of calcium phosphate ceramics. Biomaterials. 1990;11: 86–7.
43. Robinson BP, Hollinger JO, Szachowicz EH, et al. Calvarial bone repair with porous D, L-polylactide, otolaryngol. Head Neck Surg. 1995;112:707–13.
44. Itthichaisri C, Wiedmann-Al-Ahmad M, Huebner U, et al. Comparative in vitro study of human osteoblast-like cells the proliferation and growth on various biomaterials. J Biomed Mater Res A. 2007;82(4):777–87.
45. Bignon A, Chouteau J, Chevalier J, et al. Effect of micro- and macroporosity of bone substitutes on their mechanical properties and cellular response. J Mater Sci Mater Med. 2003;14:1089–97.
46. Klawitter JJ, Hulbert SF. Application of porous ceramics for the attachment of load baring orthopaedic applications. J Biomed Mater Res. 1971;2(2):161–7.
47. Padilla S, Roman J, Vallet-reqi M. Synthesis of porous hydroxyapatites by combination of gelcasting and foams burn out methods. J Mater Sci Mater Med. 2002;13(10):1193–7.
48. Chang BS, Lee CK, Hong KS, et al. Osteoconduction at porous hydroxyapatite with various pore configurations. Biomaterials. 2000;21(12):1291–8.
49. Lu JX, Flautre B, Anselme K, et al. Role of interconnections in porous bioceramics on bone recolonization in vitro and in vivo. J Mater Sci Mater Med. 1999;10(1):111–20.